ADVANCED MATERIALS
www.advmat.de

Mechanically-Tunable and Full-Color Circularly Polarized Long-Lived Phosphorescence in Chiral Superstructure Elastomers

Zhen-Peng Song, Juan Wei, Jiao Liu, Zhu-Fang Chu, Jing-Xue Hu, Susanta Chakraborty, Yun Ma, Bing-Xiang Li,* Yan-Qing Lu,* and Qiang Zhao**

Developing full-color circularly polarized organic ultralong room-temperature phosphorescence (CP-OURTP) materials with high dissymmetry factor (g_{lum}) holds significant promise for diverse optoelectronic applications. Controlling g_{lum} values is crucial for enhancing the performance and functionality of these materials, as it directly influences their chiroptical properties and potential utilities in advanced technologies. However, achieving reversible and dynamic manipulation of g_{lum} in CP-OURTP materials remains a formidable challenge. Herein, an effective strategy is presented to fabricate the chiral superstructure elastomers (CSEs) that display selective reflection colors, dynamically tunable CP-OURTP with robust g_{lum} values, full-color afterglow emissions, and superior processability within a single system. By integrating room temperature phosphorescence (RTP) polymers into the CSEs, CSEs are produced demonstrating tunable CP-OURTP with g_{lum} values switching between 0.8 and 0.15 by mechanical deformation. More importantly, these mechanochromic, programmable, and full-color CP-OURTP films enable the development of flexible and dynamic information encryption and decryption. The work provides new insights into the development of novel RTP materials and advances in their potential applications.

1. Introduction

The development of stimuli-responsive materials with dynamically tunable chiroptical properties is a key pursuit in materials science, offering immense potential for applications ranging from advanced optical devices to encrypted information storage.[1–8] Among chiroptical phenomena, circularly polarized luminescence (CPL), characterized by the emission of photons with defined spin angular momentum, stands out as particularly attractive.[9–14] Despite significant advancements in designing CPL-active materials, achieving dynamic control over the dissymmetry factor (g_{lum}), which can be used to quantify the degree of circularly polarized phosphorescence materials, remains a formidable challenge.

Long-persistent luminescence (LPL), also known as afterglow, holds important potential for applications in the optoelectronics field due to its extended emission lifetime.[15–24] Integrating LPL with CPL presents exciting opportunities for creating materials with temporally and spatially controlled chiroptical properties.[25–29] However, realizing this synergy in a stimuli-responsive platform with easily tunable g_{lum} remains very challenging and has only been reported in very few cases. Previous efforts to incorporate LPL into chiral superstructure systems have demonstrated circularly polarized ultralong organic room temperature phosphorescence (CP-OURTP), largely achieving high g_{lum} values but resulting in static g_{lum}, which limits the capability for dynamic modulation.[30–32] Ultralong phosphorescence describes the luminescence effect that persists for a duration (with a lifetime exceeding 0.1s) even after the excitation source has been turned off. Liquid crystal elastomers, known for their remarkable responsiveness to external stimuli,[33–39] present a promising platform for developing dynamically tunable CPL materials.[1,40,41] By merging the inherent chirality of chiral superstructures with the mechanical responsiveness of liquid crystal elastomers, we envision a system where g_{lum} values can be dynamically modulated by mechanical deformation. This strategy leverages the unique capability of liquid crystal elastomers for large, reversible deformations, which can directly influence the embedded chiral superstructures and consequently the emitted CPL properties.

Z.-P. Song, J. Liu, Z.-F. Chu, S. Chakraborty, Y. Ma, B.-X. Li, Q. Zhao
College of Electronic and Optical Engineering & College of Flexible Electronics (Future Technology)
Nanjing University of Posts and Telecommunications
Nanjing 210023, China
E-mail: iamyma@njupt.edu.cn; bxli@njupt.edu.cn; iamqzhao@njupt.edu.cn

J. Wei, J.-X. Hu, Y. Ma, Q. Zhao
State Key Laboratory for Organic Electronics and Information Displays & Jiangsu Key Laboratory for Biosensors
Institute of Advanced Materials (IAM)
Nanjing University of Posts and Telecommunications
Nanjing 210023, China

J. Liu, Y.-Q. Lu
National Laboratory of Solid State Microstructures & Collaborative Innovation Center of Advanced Microstructures & College of Engineering and Applied Sciences
Nanjing University
Nanjing 210093, China
E-mail: yqlu@nju.edu.cn

The ORCID identification number(s) for the author(s) of this article can be found under https://doi.org/10.1002/adma.202419640

DOI: 10.1002/adma.202419640

In this work, we introduce a novel approach to achieve mechanically tunable CP-OURTP by embedding room temperature phosphorescent (RTP) polymers within a chiral superstructure elastomer (CSE) matrix. We demonstrate that the resulting CSE-RTP composite films exhibit full-color afterglow with dynamically controllable g_{lum} values upon the application of mechanical strain. Importantly, the g_{lum} values can be reversibly modulated over a substantial range between 0.8 and 0.15, providing a simple yet powerful mechanism for controlling the degree of CPL. In contrast to the previous reports involving cholesteric liquid crystal elastomers (CLCEs),[42] our work mainly focuses on the synergistic integration of dynamic optical properties of CLCEs with RTP polymers to achieve mechanical control over CP-OURTP. While the previous literature primarily characterized the mechano-optical behavior of CLCEs, our study innovatively leverages these well-established CLCE optical properties as a dynamic platform to manipulate and tune the chiroptical emission of RTP materials. The CSE-RTP films exhibit remarkable optical properties due to their stimulus-responsive helical nanostructure changes in response to mechanical stretching deformations. To gain a better understanding of the optical characteristics of the intrinsically stretchable CSE-RTP films, various optical conditions are meticulously investigated. The overall reflection changes with the applied strain due to the reorientation of the LC director under mechanical stretching. This dynamic control is made possible by the intimate coupling between the macroscopic deformation of the liquid crystal elastomer (LCE) and the microscopic alignment of the chiral LPL emitters within the helical superstructure. Moreover, we present the potential of these CSE-RTP films for advanced anti-counterfeiting applications by showcasing a multi-level encryption strategy based on reflection colors, fluorescence, long-lived phosphorescence, circular polarization characteristics, and mechanically modulated full-color afterglow. This work not only introduces a novel class of mechanically tunable CP-OURTP materials but also opens new pathways for developing next-generation chiroptical devices with unprecedented control over light polarization.

2. Results and Discussion

2.1. Material Design and Characterization

The freestanding CSE-RTP films consist of the polymerizable LC monomer RM257 (71.2 wt.%), chiral dopant LC756 (3.2 wt.%), dipropylamine (DPA, 0.25 wt.%), photoinitiator of Irgacure 651 (0.55 wt.%), cross-linker PETMP (4.8 wt.%), chain extender EDDET (18.5 wt.%) and RTP polymer P3 (1.5 wt.%) (**Figure 1a**). The reason these materials were chosen is that the resulting CSE films exhibit a consistent structural color and a wide range mechanochromic response to strains across the entire visible spectrum. As a result, the reflection spectra of the CSE films can be dynamically manipulated by mechanical deformation, enabling them to effectively overlap with the emission peaks of various RTP polymers and achieve high g_{lum} values. RTP polymers with different afterglow emissions were specifically selected instead of RTP molecules because the interactions between polymer chains can effectively limit the molecular motions of RTP molecules, thereby suppressing nonradiative relaxation pathways and leading to persistent lifetimes and high quantum efficiencies. Moreover, the polymer networks in CSEs offer a rigid mechanical structure that stabilizes the triplet excitons of RTP molecules, further reducing the nonradiative decay and quenching factors like triplet oxygen. The synthesis procedures of RTP polymers are shown in Experimental procedures (Figures S1–S13, Supporting Information). Specifically, the chiral dopant LC756 was selected to alter the reflection colors of the developed CSE. DPA was chosen to initiate the first-stage reaction between thiols and diacrylates. Irgacure 651 was used as a photoinitiator to trigger a subsequent second-stage photocross-linking, thereby making the CSE-RTP structure stable and permanent. The cross-linker PETMP was to bound LC mesogens to the mechanical framework of the network, enabling robust and repeatable shape changes. The precursor mixture in dichloromethane (CH_2Cl_2) solvent was transferred into a cleaned glass dish, allowing the solvent to evaporate completely under ambient conditions, and then irradiated with 365 nm UV light (50 mw/cm^2) for 10 min to initiate the final photoinitiated cross-linking. As a result, the CSE-RTP film with the desired red reflection color was obtained with the approximate thickness of 150 μm.

Compared to the previously reported literatures, there are three distinct advantages in the preparation of the CSE-based CP-OURTP materials. First, by integrating RTP polymers into the CSEs, we successfully developed dynamically tunable CP-OURTP materials that exhibit robust g_{lum} values, full-color afterglow emissions, and excellent processability, all within a single system. This approach only requires 2 h at room temperature to produce the reflective surface of the CSE-RTP films. In contrast, in previous studies, the CLCEs were usually obtained at a high temperature of 80 °C for 20 h to ensure the full completion of the Michael addition reaction.[40] Second, the approach we employed is straightforward yet highly efficient, demonstrating excellent reproducibility and scalability for the production of uniformly colored, large-area CSE-RTP films. Thirdly, the LC materials used for the fabrication of the CSE-RTP films are all commercial chemicals and the resulting CSE-RTP films exhibit a consistent structural color and a wide-ranging mechanochromic response to strains throughout the entire visible spectrum. The RTP polymers with different afterglow emissions were specifically chosen instead of small phosphorescence molecules because the interactions among polymer chains can effectively restrict the molecular motions of RTP molecules, thereby suppressing nonradiative relaxation pathways and resulting in persistent lifetimes and high quantum efficiencies. Additionally, the polymer networks in CSEs provide a rigid mechanical structure that stabilizes the triplet excitons of RTP molecules, further reducing the nonradiative decay and quenching factors such as triplet oxygen. The processability of the CSE-RTP films was better than that of the bilayered soft helical superstructure. In addition, the preparation of scalable CP-OURTP materials was not possible due to the limitation of the LC glass substrates in previous literature. Furthermore, the approach we employed is straightforward yet highly efficient, enabling uniformly colored, large-area CSE-RTP films.

Five types of the CSE-RTP films were fabricated by changing the content of the chiral agent and the types of RTP polymers.[8,31,43] The CSE-RTP films were defined as CSE-R-P1, CSE-R-P2, CSE-R-P3, CSE-G-P2, and CSE-B-P1, respectively, based on their reflection colors (indicated by the middle letter, "R"

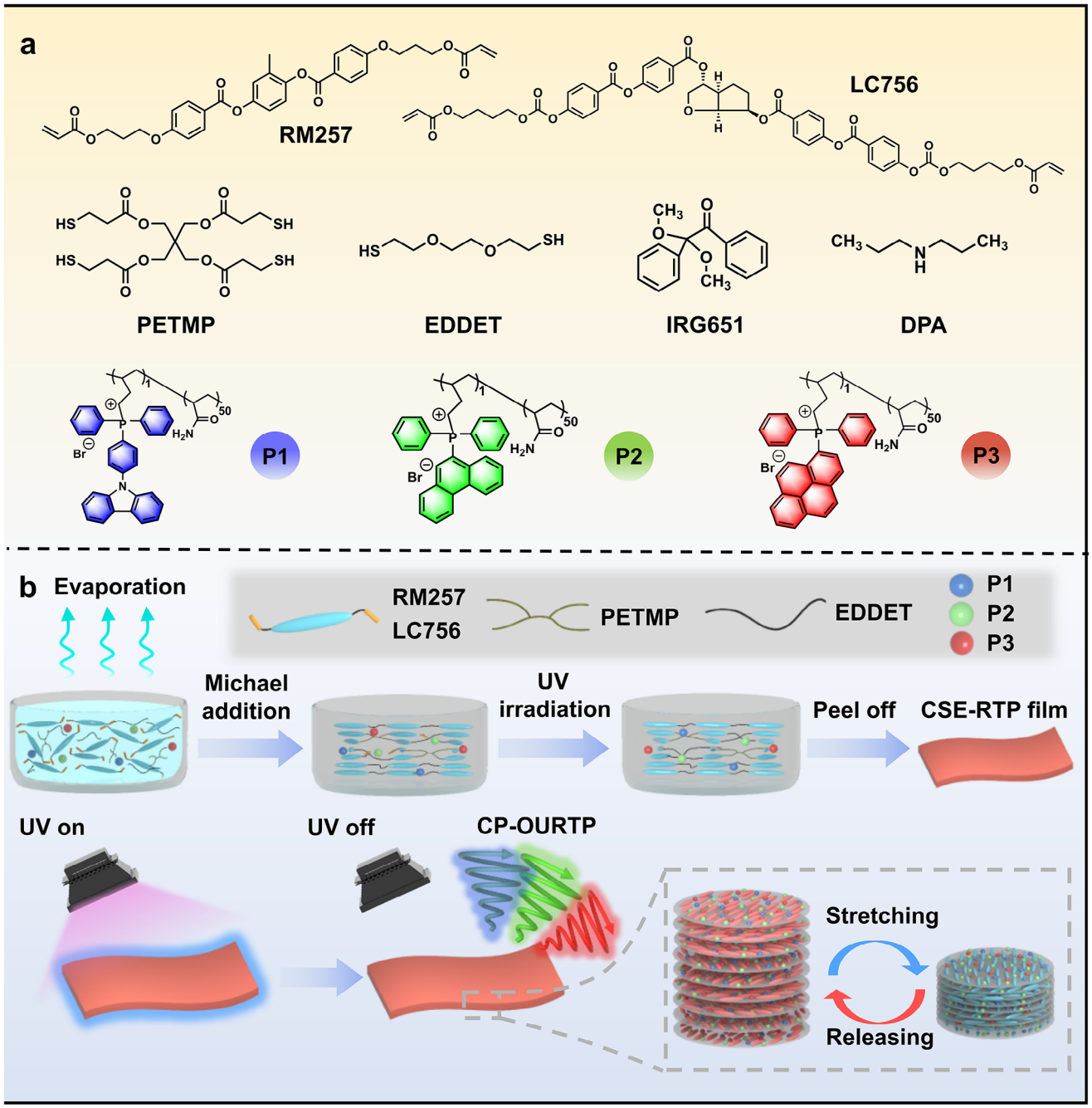

Figure 1. Fabrication of circularly polarized organic ultralong room-temperature phosphorescence (CP-OURTP) materials. a) Chemical structure of fabricating CP-OURTP materials composed of diacrylate mesogen (RM257), chiral dopant (LC756), cross-linker (PETMP), chain extender (EDDET), photoinitiator (Irgacure 651), dipropylamine (DPA), and room temperature phosphorescence (RTP) polymers (P1, P2, and P3). b) Schematic illustration of fabricating mechanically-tunable CP-OURTP materials based on chiral superstructure elastomer (CSE)-RTP films.

is red, "G" is green, and "B" is blue) and the types of RTP polymers (described by the last letter, P1, P2, and P3). The CSE-RTP films with red, green, and blue reflection colors can be obtained by controlling the concentration of the chiral dopant LC756 at 3.2, 3.8, and 4.2 wt.%, respectively. More information can be found in Figures S14–S16 and Table S1 (Supporting Information). The obtained CSE-RTP films demonstrate a consistent color and a vertically aligned helix, despite the absence of other treatments such as alignment layer, magnetic or electric fields, or centrifugation. An important factor is the formation of the gel during the polymerization process of thiols and acrylates: the gel produced in the reaction adheres so firmly to the substrates that it is unable to shrink laterally as the solvent evaporates, which is evident from the unchanged surface of the films during drying. This prevents the deswelling from occurring in any directions except vertical (z), causing the LC director to orient along the glass

substrates and consequently resulting in a vertical helix axis along the z direction.[44] A schematic of cholesteric networks, with the helical axis aligned along the solvent evaporation direction, can be found in Figure S17 (Supporting Information).

2.2. Photophysical Properties of RTP-CHS Films

The resulting CSE-RTP films exhibit remarkable mechanochromic behavior. **Figure 2a** depicts the schematic process of an initially red-reflecting CSE-R-P3 film that was uniaxially stretched perpendicularly to the helix axis, whose reflection colors shifted from red to green and finally to blue. To verify the uniform distribution of RTP polymers in CSE, we conducted an experiment of energy-dispersive X-ray spectroscopy (EDS) mapping on CSE-R-P3 film (Figure S18, Supporting Information). The result revealed that RTP polymer (P3) was well dispersed in CSE. Initially, the CSE-R-P3 film exhibited a uniform red structural color. As the strains were applied from 0 to 100%, the reflection color of the CSE-R-P3 film sequentially changed from red to green to blue (Figure 2b; Figure S16, Supporting Information). Notably, the film could revert to its initial state after releasing the strains (Figure 2b; and Movies S1–S3, Supporting Information). Interestingly, a significant difference exists between the top and bottom for CSE-R-P3 film after it was detached from the glass dish (Figure S19, Supporting Information). To determine whether this is related to the heterogeneous polymerization due to a different photo-illumination situation between the top and bottom of the films, we conducted the experiments where the polymerization induced by UV light was controlled from the bottom side of the glass substrate. Subsequently, the photographs from the top and bottom sides of the CSE-R-P3 film under no CPF, L-CPF and R-CPF were captured, respectively (Figure S20, Supporting Information). The results indicate that the photo-illumination either from the top or the bottom of the glass substrates does not lead to a significant difference. The same phenomenon was also observed in the CSE-R-P1 and CSE-R-P2 films (Figures S21 and S22, Supporting Information). The bottom side of the CSE-RTP films, which was directly in contact with the glass substrates during the reaction, displays no selective reflection and scatters light intensely, resulting in a colorless appearance. This is possibly due to the fact that the solvent evaporation is obstructed by the glass substrates, which prevents the unidirectional compression on the underside of the CSE-RTP films during their formation. Furthermore, the CSE-R-P3 film displays a red color in its initial state when observed through a right-handed circularly polarized filter (R-CPF) and appears dark through a left-handed circularly polarized filter (L-CPF), indicating the presence of a right-handed chiral superstructure (Figure 2c; Figure S16, Supporting Information). UV-Visible (UV−vis) absorption peaks of CSE-RTP film are located at 250 and 350 nm, respectively, primarily originating from the $\pi \rightarrow \pi^*$ and n $\rightarrow \pi^*$ transitions of RTP polymers (Figure 2d). The CSE-R-P3 film displays a positive Cotton effect at ≈300 nm as shown from circular dichroism (CD) spectrometer, further confirming the right-handed helical superstructure of CSE-R-P3 film (Figure 2e). To better understand the mechanochromic property of CSE-R-P3 film, the qualitative analysis was performed with POM and wide-angle X-ray diffraction (WAXD). From the POM images, the oily streak textures of the CSE-R-P3 film were not clearly visible (Figure 2f; Figure S23, Supporting Information) due to the lack of well-aligned cholesteric phase evidence. Microscopically, the film displays the grain-like textures.[44,45] Generally, the oily streak textures in CLCEs can be observed in a well-aligned cholesteric phase with a certain thickness of LC cells. For example, Guo et al.[40] reported that the CLCE film exhibited oily streak textures in a well-aligned planar LC cell with the cell thickness of 50 µm. Suk-kyun Ahn et al.[46] prepared a direct ink writing (DIW)-based 3D-printable CLCE that showed the oily streaks by the shear-induced alignment. The WAXD patterns change from the shape of a ring to the arcs in the transverse direction (Figure 2f), indicating that the red-reflecting CSE-R-P3 film possesses a polydomain structure, while the stretched blue-reflecting CSE-R-P3 film exhibits a monodomain structure. The stretched CSE-R-P3 film with monodomain shows a periodic transition from dark to bright field when rotated at 45° intervals in the POM images, confirming that the LC director primarily aligns along mechanical stretching direction (Figure S24, Supporting Information).[35,44,47] The CSE-RTP films were photopolymerized with UV light to initiate an acrylate homopolymerization to stabilize the cholesteric phase, but this process caused haze due to the cross-linking and randomness in alignment.[45] Haze (H) is an optical phenomenon resulting from light scattering. In the initial state, the CSE-RTP films have polydomain structures, where the LC directors rotate periodically with stretchable components, such as chain extenders and cross-linkers. When the strain is applied, the LC directors tend to align along the direction of mechanical stretching, resulting in the formation of quasi-monodomain structures.[42] When the quasi-monodomains of the CSE-RTP films are formed by mechanical stretching deformation, the light scattering can be reduced, as confirmed by the H measurement. The experimental setup for the H measurement is shown in Figure S25 (Supporting Information). The total transmittance (T_t) is the sum of the diffuse transmittance (T_d) and the specular transmittance (T_s). The H can be calculated by the equation $H = T_d/T_t$.[48] The results clearly show that the high H (%) decreases with the applied strain and the CSE-R-P3 film transitions to a visibly blue appearance, directly correlating with the reorientation of the cholesteric phase and reduce scattering (Figure S25, Supporting Information). Additionally, the reflection spectra of CSE-R-P3 film were investigated at various strains under no polarizer, L-CPF, and R-CPF, respectively (Figure 2g–i). In the initial state, the reflection of the CSE-RTP under R-CPF reaches a maximum of only 25%, which is similar to earlier observations.[35,40,41,44] This lower-than-ideal initial reflectance under R-CPF, and the subsequently observed maximum of only 12% under L-CPF in the stretched state (Figure 2h), can be attributed to a combination of factors, primarily related to the non-ideal nature of real CLCE materials compared to theoretical models. First, the inherent polydomain structure of our cross-linked CSE-RTP films significantly contributes to light scattering, which reduces the specular reflection intensity. While photopolymerization stabilizes the cholesteric phase, the resulting network inevitably contains domain boundaries and orientational disorder. These imperfections act as scattering centers, leading to diffuse reflection and a loss of intensity in the specularly reflected beam that we measure.[47] Second, variations

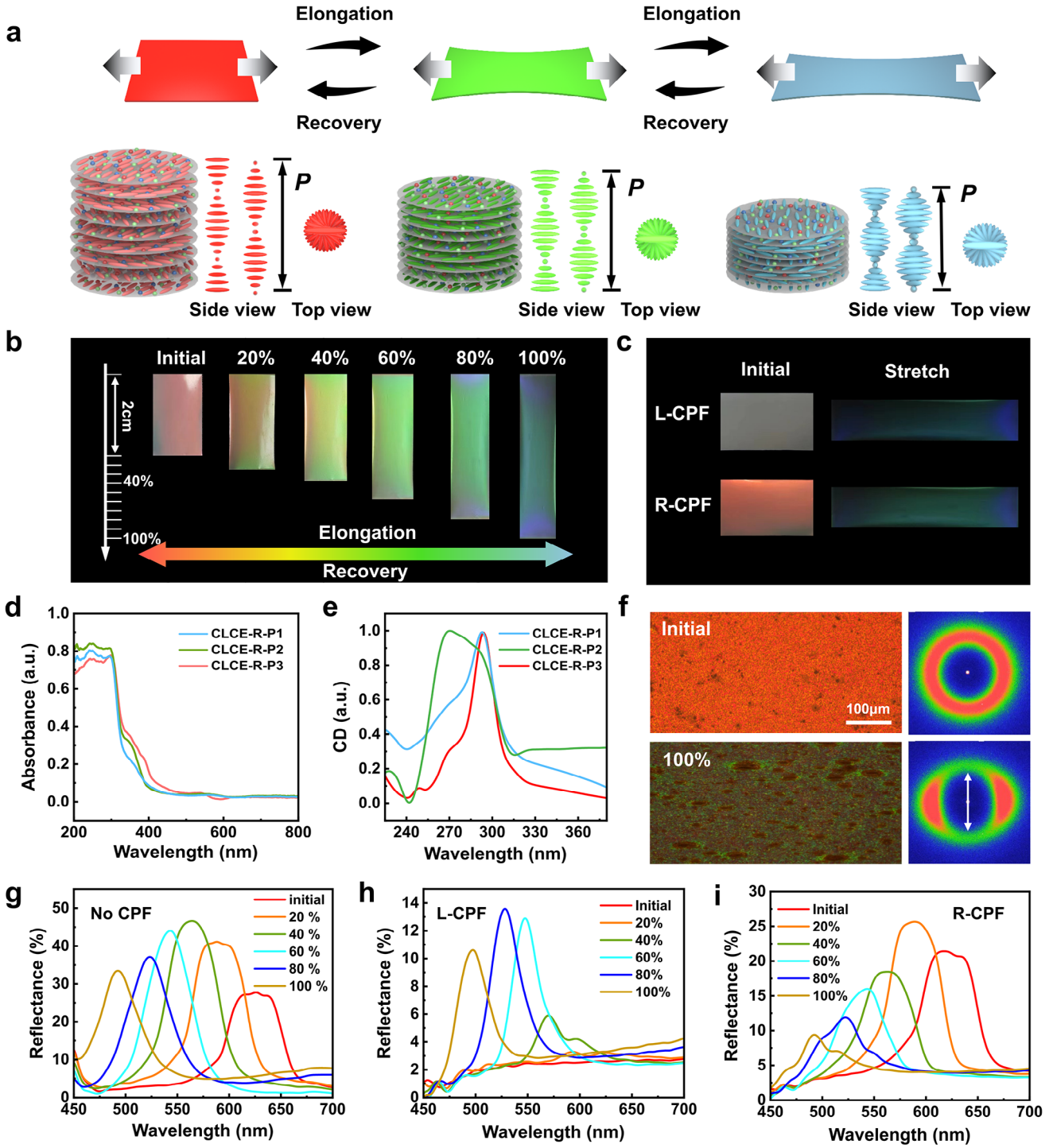

Figure 2. Chiroptical properties of CSE-RTP films. a) Schematic process of fabricating CSE-RTP films with different reflection colors by stretching and releasing. b) Photographs of CSE-R-P3 film ("R" signifies red reflection) being mechanically stretched, with reflection colors changed from red to blue at different strains. c) Photographs of CSE-R-P3 film in the initial state and stretched state under left-handed circularly polarized filter (L-CPF) and right-handed circularly polarized filter (R-CPF), respectively. d) Absorbance spectra and e) Circular dichroism (CD) spectra of CSE-R-P3 film in the initial state. f) Reflection polarized optical microscope (POM) images in the initial state and stretched state under no CPF and the corresponding wide-angle X-ray diffraction (WAXD). g–i) Reflection spectra of CSE-R-P3 film at different strains under no CPF, L-CPF and R-CPF, respectively.

in helical alignment and film thickness across the measured area likely further contribute to the reduced reflectance. Even with controlled fabrication, real films can exhibit slight non-uniformities. The reflection from a cholesteric liquid crystal is highly sensitive to the helical pitch and alignment. If the helical pitch or director alignment deviates slightly across the illuminated area, or if the film thickness is not perfectly uniform, the reflected intensity will be averaged out and reduced compared to a perfectly uniform, monodomain film. This averaging effect, combined with the polydomain scattering, results in the observed initial R-CPF reflection of 25% being lower than the idealized 50%. Regarding the maximum reflection of only 12% under L-CPF in the stretched state (Figure 2h), this is lower than the initial R-CPF reflection due to the imperfect unwinding of the helix and the remaining structural disorder, even at high strains. While stretching unwinds the helix and transitions the reflection towards the left-handed channel, the process is not perfectly controlled, and some degree of polydomain character and alignment imperfections likely persist even at 100% strain. Furthermore, the transition to a Bragg reflector-like state, as the helix unwinds, implies that the reflection becomes less specifically circularly polarized, and more broadly reflective of both polarizations, but not necessarily with high intensity in either channel due to the aforementioned scattering and non-idealities. Therefore, the observed reflection maxima of 25% (initial R-CPF) and 12% (stretched L-CPF) are realistic values for cross-linked CLCE films, reflecting the inherent complexities and non-idealities of real materials, and are consistent with previously reported experimental observations. After polymerization, the reflection color of CSE-R-P3 film displays no obvious changes to the naked eyes (Figure S26, Supporting Information), while the reflection peak undergoes a slight blue shift from 652 to 648 nm ($\Delta\lambda \approx 4$ nm) (Figure S27, Supporting Information). It is observed that the reflectance spectra undergo a significant blue shift under no CPF, with the reflection center moving from 628 to 490 nm ($\Delta\lambda \approx 138$ nm) as the strains increase (Figure 2g; Figure S28, Supporting Information), due to the reduced thickness of CSE-R-P3 film. A similar phenomenon is detected in the reflection spectra of CSE-R-P1 and CSE-R-P2 films (Figures S29 and S30, Supporting Information). When the deformation is less than 40%, the reflectance of CSE-R-P3 under no CPF increases with the elongation due to the planar orientation (Figure 2g). When the deformation exceeds 40%, the structure of CSE-R-P3 film gradually transforms from a helical to a stratified structure, resembling a 1D Bragg reflector (Figure 2g–i).[44,49]

To gain a better understanding of how the intrinsically stretchable nature of CSE-RTP films dictates their optical characteristics, we have investigated various optical conditions, directly correlating them with the molecular rearrangements induced by mechanical strain. The overall reflection changes with the applied strain are fundamentally driven by the reorientation of the LC director at the molecular level under mechanical stretching. In the initial state, the CSE-RTP films have polydomain films, characterized by periodically rotating LC directors and inherent disorder due to stretchable components, resulting in a broad reflection band and relatively low circular polarization selectivity. When the strain is applied, the LC directors undergo a coordinated reorientation, tending to align along the direction of mechanical stretching. This molecular alignment leads to the formation of quasi-monodomain structures, which in turn sharpens the reflection band and shifts it to shorter wavelengths (blue shift), manifesting as the observed mechanochromism. Initially, with right-handed helical ordering, the unstretched CSE-R-P3 film preferentially reflects right-handed circularly polarized light, exhibiting color reflection primarily under R-CPF at low strains (<40%). As the length strain exceeds 40%, and with increasing strain, the helix unwinding at the molecular level becomes progressively more pronounced. This unwinding is directly responsible for the gradual appearance and increasing prominence of the reflection spectrum under L-CPF, while the reflection under R-CPF diminishes. (Figure S16, Supporting Information). Ultimately, at high strains, the strain-controlled CSE-R-P3 films approach a stratified, Bragg reflector-like structure at the molecular level, losing circular polarization selectivity. This molecular transition from a helical cholesteric structure to a stratified Bragg reflector structure explains the observed decrease in g_{lum} values of CP-OURTP, as the material loses its ability to selectively filter circularly polarized light.

To further elucidate the molecular mechanism of helical structure deformation, the POM images of the CSE-R-P3 film were captured at azimuthal angles with every 45° in the initial state, 15% stretched state, and 50% stretched state, respectively (Figure S31, Supporting Information). Initially, the average refractive indices of the CSE-R-P3 at all azimuth angles are circularly uniform, thereby resulting in the same color as shown by POM. When the CSE-R-P3 films are stretched by 15%, the LC molecules are fixed at 90° and 270°, which are perpendicular to the stretching direction. In this case, the LC molecules begin to unwind in the direction parallel to the applied strain, while the molecules with the director perpendicular to the strain remain fixed. Therefore, it shows almost the same colors at (0°, 180°) and (90°, 270°) from POM images. In contrast, the images captured at (45°, 225°) and (135°, 315°) exhibit different colors. When the CSE-RTP films are stretched by 40%, the LC molecules perpendicular to the applied strain start to unwind. After exceeding the critical strain, all LC molecules align with the applied strain direction, resembling monodomain structures, and the helical structures are disrupted. It is found that the POM images are different when the azimuthal angles are parallel and perpendicular to the stretching direction. Additionally, the POM at 45° and 135° show the same color due to the identical average refractive indices at every 45° from the stretching direction. Therefore, the POM images provide visual confirmation of the strain-induced molecular rearrangements of LC directors and the transition from a polydomain cholesteric structure to a quasi-monodomain or stratified structure, directly correlating with the observed changes in reflection and CPL properties. Furthermore, the photographs, reflection spectra, and CPL characterization of the aggregation-induced emission dye (1,1,2,3,4,5-Hexaphenylsilacyclopenta-2,4-diene, HPS)-doped CSE film under no CPF, L-CPF, and R-CPF were also conducted (Figures S32 and S33, Supporting Information). The observed g_{lum} variations are consistent with the results from the CSE-R-P3 film. Moreover, the stretching-releasing cycles were performed more than 20 times with no obvious degradation (Figure S34, Supporting Information). Meanwhile, the blue shift in the wavelength was observed, shifting from 659 to 459 nm, as the content of LC756 increased from 3.2 to 4.3 wt.% (Figure S35, Supporting Information).

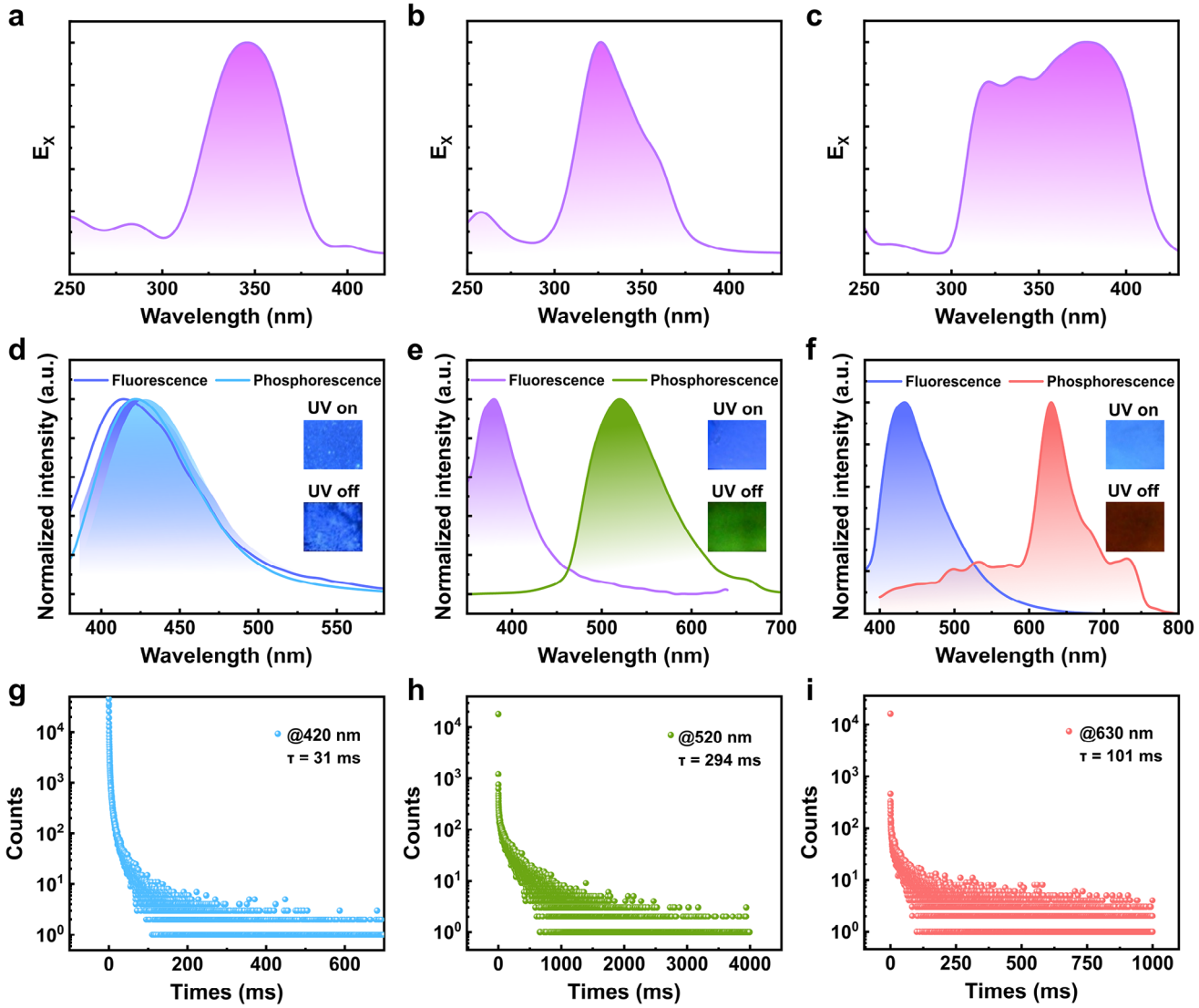

Figure 3. Photophysical properties of CSE-RTP films. a–c) Excitation spectra of CSE-R-P1 film (a), CSE-R-P2 film (b), and CSE-R-P3 film (c). d–f) Photoluminescent (PL) emission spectra and delayed PL spectra of CSE-R-P1 (d), CSE-R-P2 (e), and CSE-R-P3 (f) (inset photographs of CSE-R-P1, CSE-R-P2, and CSE-R-P3 films taken under 365 nm UV light on and off). g–i) Phosphorescent lifetimes of CSE-R-P1(g), CSE-R-P2 (h), and CSE-R-P3 films (i).

To gain further insights into the photophysical properties of CSE-RTP films, we performed the photoluminescence (PL), decay time, and PL quantum yields measurements. The normalized excitation spectra, the normalized steady-state photoluminescence spectra, delayed PL spectra, and lifetime curves of CSE-R-P1, CSE-R-P2, and CSE-R-P3 films were determined, respectively. The PL spectra can reflect the luminescent colors of CSE-RTP materials. Under irradiation with 365 nm UV light, these CSE-RTP films emit blue color. Intriguingly, these CSE-RTP films with bright blue, green, and red afterglow emissions are visible to the naked eyes after removing UV light source (insets in **Figure** 3d–f), which are very attractive in practical applications. The CSE-RTP films exhibit strong phosphorescent emissions at 420, 520, and 630 nm, respectively (Figure 3d–f). Furthermore, PL quantum yields of CSE-RTP are determined to be 6.86% for CSE-R-P1, 1.97% for CSE-R-P2, and 9.47% for CSE-R-P3, respectively (Figure S36, Supporting Information). Additionally, the lifetimes of CSE-R-P1, CSE-R-P2, and CSE-R-P3 are 31 ms with an emission peak at 420 nm, 294 ms at 520 nm, and 101 ms at 630 nm (Figure 3g–i). It is noteworthy that the emission lifetime of the CSE-RTP film decreases to 84% of its original value after the mechanical stretching (Figure S37, Supporting Information). The organic quaternary phosphonium derivatives show RTP as a result of intermolecular electronic coupling induced by proximity within the rigid environment. In these derivatives, the aromatic groups are directly attached to the phosphorus center, forming a characteristic molecular rotor. Crucially, the generation of RTP is mainly attributed to the ability of polyacrylamide network within the CSE to effectively immobilize these phosphors, thereby suppressing non-radiative decay pathways such as molecular rotations and vibrations.

When these CSE-RTP films are stretched, the strains applied to the polymer chains disrupt the immobilization of phosphors, finally resulting in a decrease in emission lifetimes and RTP intensity.[17] The CSE-R-P1 shows no obvious color change before and after UV irradiation, which is consistent with the overlap of fluorescence and phosphorescence spectra. The CSE-R-P2 film emits sky blue fluorescence under UV irradiation and then transforms to green phosphorescence after ceasing irradiation, displaying the most persistent visualization of ≈1.5 s among these three developed films. The CSE-R-P3 film shows a different transformation from sky blue to red after ceasing UV irradiation, with luminescence lasting for 0.5 s.

2.3. Optical-Mechanical Responsiveness of CSE-RTP Films

Right-handed CSE-RTP films are capable of reflecting right-handed circularly polarized light while permitting left-handed circularly polarized light to pass through. When the PBGs of CSEs are partially or fully aligned with the emission peaks of RTP polymers, the excited right-handed CPL is reflected, whereas the left-handed CPL is transmitted. Therefore, the right-handed CSEs produce a left-handed CPL (**Figure** 4a). When irradiated by 365 nm UV light, the fabricated CSE-RTP films exhibit a blue emission. More intuitively, after ceasing UV irradiation, the afterglow of CSE-RTP films in the initial state and stretched state are visible to the naked eyes at room temperature with blue emission for CSE-R-P1, green for CSE-R-P2, and red for CSE-R-P3 films, respectively. The full-color emissions of CSE-RTP films in the initial state and stretched state were recorded under no CPF, under L-CPF, and R-CPF conditions, respectively (Figure 4b; Figures S38–S40 and Movies S4–S7, Supporting Information). Compared to the previous study, the key novelty lies in extending the application of stretchable CLCEs from solely manipulating reflection colors to dynamically controlling the circularly polarized phosphorescence emission of embedded functional materials. The photographs of the phosphorescence emissions of the CSE-R-P1, CSE-R-P2, and CSE-R-P3 films under L-CPF and R-CPF, both before and after stretching at different strained states, were captured to provide a thorough understanding of how the CP-OURTP and their optical properties evolve under different stretching conditions. The observed changes in phosphorescence properties of the strain-induced CSE-RTP films are fundamentally governed by the molecular rearrangements within the CLCE matrix upon mechanical deformation. First, the strain-induced polydomain-to-monodomain transition, driven by LC director reorientation at the molecular level, directly influences the observed phosphorescence emission intensity under different circular polarizer filters. In the initial polydomain state, the right-handed helical structure preferentially reflects right-handed circularly polarized light, leading to more pronounced phosphorescence emission under L-CPF compared to R-CPF at lower strains, as L-CPF is transmitted while R-CPF is partially reflected (Figure 4b; Figures S38–S40, Supporting Information). As strain exceeds 40% and the helix progressively unwinds at the molecular level, transitioning towards a stratified structure, the material loses its circular polarization selectivity (Figures S38–S40, Supporting Information).[50] Consequently, the phosphorescence emission becomes comparable under both L-CPF and R-CPF, reflecting the molecular transition to a less chiral ordered state. Second, the strain-induced shift in the CPL emission wavelength (Figure 4d) and the associated variations in g_{lum} values are also a direct consequence of molecular rearrangements within the CLCE matrix. The initial high g_{lum} value of CP-OURTP, achieved when the photonic bandgap (PBG) of the CSEs overlaps with the RTP emission band (Figure 4c), is due to the chiral amplification effect of the ordered helical structure. However, as stretching induces helix unwinding and the transition toward a stratified structure at the molecular level, the PBG shifts (Figure 4d), and the chiral ordering is disrupted. This molecular-level structural change directly leads to the observed decrease in g_{lum} values, as the material loses its ability to selectively emit circularly polarized phosphorescence. The low g_{lum} value of 0.15 in the stretched state (Figure 4e) further confirms the near disappearance of the helical structure and the loss of circular polarization selectivity at the molecular level. Third, and importantly, the decrease in emission lifetime upon stretching (Figure S37, Supporting Information) is also intrinsically linked to molecular rearrangements that alter the microenvironment of the RTP phosphors. The mechanical strain disrupts the rigid immobilization of phosphors within the CLCE network by inducing polymer chain elongation, increased free volume, and enhanced molecular mobility. This loosening of the molecular cage surrounding the RTP emitters increases non-radiative decay pathways, resulting in the observed reduction in emission lifetime. In summary, the entire suite of observed RTP emission property changes, intensity under CPF, g_{lum} value/CPL, emission wavelength, and lifetime, are all directly and mechanistically correlated with the molecular rearrangements within the CSE-RTP films induced by mechanical stretching.

To measure the degree of CPL, the g_{lum} is defined as: $g_{lum} = 2(I_L - I_R)/(I_L + I_R)$. Here, I_L and I_R denote the intensities of left- and right-handed circularly polarized light, respectively. The g_{lum} values vary from -2 to +2, with -2 representing completely right-handed circularly polarized light and +2 signifying purely left-handed circularly polarized light.[2,3,7,10,13,41] While the CSE-R-P3 film exhibits a respectable initial g_{lum} value of ≈0.8, which is indeed comparable to the maximum g_{lum} values reported for fluorochromic CLCEs in previous literature,[41] it is important to recognize that achieving a perfect g_{lum} value of 1.0 in solution-processed, cross-linked CLCE films is inherently challenging due to fundamental material limitations, even with meticulous preparation. The fact that our initial g_{lum} value is less than unity, despite careful fabrication, does not indicate a deficiency in material quality, but rather reflects the inherent polydomain nature and unavoidable structural imperfections present in real-world CLCE elastomers. The cross-linking process, while essential for creating the elastomeric network, intrinsically introduces a degree of quenched disorder and polydomain structure into the cholesteric phase. Even in well-optimized preparations, perfect monodomain alignment across macroscopic areas is practically unattainable in these solution-processed systems. This inherent polydomain character inevitably leads to some degree of light scattering and imperfections in the circular polarization purity of the reflected light, even in the initial, pre-stretched state.[47] Furthermore, while a larger thickness of the CSE-R-P3 film is beneficial for enhancing overall reflection intensity, it can also introduce greater variability in helical alignment and pitch through the film thickness.[45] This alignment variability, even if minor,

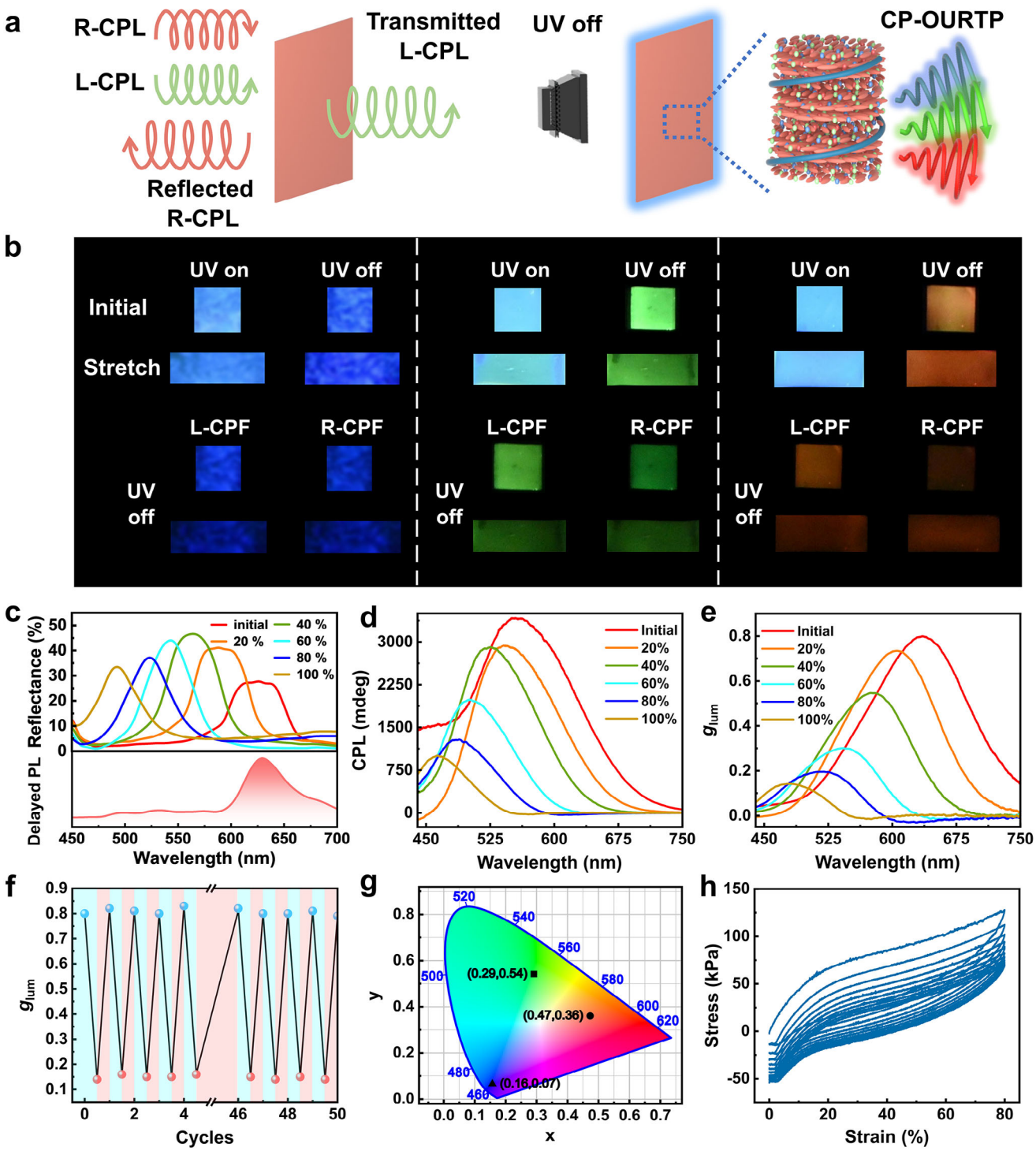

Figure 4. Phosphorescent properties and dynamically tunable CSE-RTP films. a) Schematic diagram of CP-OURTP generated by CSE-RTP films. b) Photographs of CSE-R-P1, CSE-R-P2, and CSE-R-P3 films under 365 nm UV on and off, and under L-CPF and R-CPF before and after stretching. c) Delayed Photoluminescence (PL) spectra of P3, and the reflection spectra of the CSE-R-P3 under different strains. d) Circularly polarized luminescence (CPL) spectra of CSE-R-P3 film being mechanically stretched at various strains (from 0% to 100%). e) g_{lum} curves at different strains of CSE-R-P3 film. f) Reversible changes of g_{lum} values against repeated stretching and releasing cycles of CSE-R-P3 film. g) CIE coordinates afterglow emissions from CSE-R-P1, CSE-R-P2, and CSE-R-P3 films. h) Hysteresis curves of CSE-R-P3 film obtained from repeated load and unload tests at a linear strain rate of 2% min^{-1} up to 80% strain.

further contributes to a reduction in the overall circular polarization purity of the reflected light and, consequently, a g_{lum} value below the ideal 1.0. The g_{lum} value, by definition, is a direct measure of the material's ability to selectively filter circularly polarized light. A g_{lum} value of 0.8 indicates that while the CSE-R-P3 film exhibits significant circular polarization selectivity and efficient CP-OURTP, it is not a perfect circular polarizer. The slight discrepancy in reflectivity between left- and right-handed circularly polarized light, as reflected in the g_{lum} value of 0.8, is therefore a consequence of the inherent structural characteristics of realistic, solution-processed CLCE films, rather than a reflection of poor preparation quality. The similar variation of g_{lum} is observed for CSE-R-P2 film (Figure S42, Supporting Information), while for CSE-R-P1 film, the g_{lum} exhibits a gradual increase from 0.35 to 0.40, and then decreases with the increased applied strains (Figure S43, Supporting Information). The maximum g_{lum} values in CSE-RTP films are not located at the position where the PBGs and the emission peaks of RTP are overlapped, indicating that the polarization degree of CPL is independent of the position of the PBGs.[5]

The CSE-R-P2 film demonstrates a non-monotonic relationship between RTP content and emission intensity (Figure S41, Supporting Information). This behavior, characterized by an initial sharp increase followed by a plateau and subsequent decrease, can be explained by a combination of competing factors related to the microenvironment and dispersion of the RTP polymer P2 within the CSE matrix. The initial significant enhancement in RTP emission from 1 to 2 wt.% is primarily attributed to the creation of an increasingly favorable rigid microenvironment for RTP emission as more P2 polymer is incorporated into the CSE matrix. In contrast to small molecule RTP emitters, we strategically employed RTP polymers (P2) which, due to their polymeric nature and chain entanglement within the CSE network, exhibit inherently restricted molecular motions. Furthermore, within the CSE-R-P2 composite, a range of intermolecular interactions (ionic, ion-dipole, and dipole-dipole) are expected to occur between the LC molecules of the CSE and the RTP polymer chains. These interactions facilitate the effective dispersion of the RTP polymer chains within the CSE architecture at lower concentrations, without disrupting the underlying LC arrangement of the CSE. This well-dispersed RTP polymer within the rigid CSE network effectively restricts the molecular motions of the phosphorescent moieties, thereby suppressing non-radiative relaxation pathways such as molecular rotations and vibrations and consequently leading to enhanced phosphorescence emission intensity and potentially longer lifetimes. Moreover, the polymer network of the CSE itself provides an inherently rigid mechanical structure that further stabilizes the triplet excitons of the RTP molecules, reducing non-radiative decay and quenching processes, including triplet oxygen quenching, by effectively limiting oxygen diffusion into the rigid matrix.[17] However, as the content of P2 is increased further, beyond 2 wt.% and especially exceeding 5 wt.%, the dispersion of the RTP polymer within the CSE matrix becomes less uniform. At these higher concentrations, aggregation of the P2 polymer chains is likely to occur, leading to inhomogeneities in the luminescence and increased self-quenching effects. This deterioration in dispersion and onset of self-quenching counteracts the benefits of increased RTP concentration, resulting in the plateauing of emission intensity between 2 and 5 wt.%, and the subsequent decrease observed at 8 wt.% P2. Therefore, while increasing RTP content initially enhances emission by creating a more favorable rigid microenvironment and restricting molecular motions, achieving optimal RTP performance requires a delicate balance to maintain good dispersion and avoid concentration quenching effects at higher loadings.

The stretching-releasing cycles of g_{lum} in the initial and stretched state were performed over 50 times without fatigue under the same test conditions (Figure 4f), proving its reusable characteristic. We also investigate how the thickness of the CSE-R-P3 film affects the g_{lum} values. The results indicate that the g_{lum} curves almost stay the same when the film thickness is between 100 and 200 µm. However, as the thickness reaches 250 µm, the g_{lum} values of the CSE-R-P3 film start to decrease (Figure S44, Supporting Information). In addition, the CPL spectra at various strains were also measured, showing the g_{lum} variation in the range of 0.52 to 0 for the CSE-B-P1 film and 0.42 to 0.03 for the CSE-G-P2 film (Figures S45 and S46, Supporting Information). Moreover, each scale of the luminescence spectra is plotted by drawing the points that are consistent with their phosphorescent spectra on the CIE (1931) chromaticity diagram. The luminescent colors of the CSE-RTP films generate a bathochromic shift from blue (0.16, 0.07) through regions near green (0.29, 0.54) and finally to red (0.47, 0.36) (Figure 4g). Notably, the CSE-R-P3 film exhibits excellent stretching characteristics and long lifetime RTP, which is specifically selected for further investigation of dynamically tunable CP-OURTP properties. The CSE-RTP films are stretchable material with excellent mechanical performance. The stress–strain curves show that the elongation at break of the CSE-R-P3 is 110% with the measured modulus of 0.88 Mpa (Figure S47, Supporting Information). The load-unload stress response of the CSE-R-P3 film exhibits constant hysteresis when stretched up to a maximum of 80% (Figure 4h). Furthermore, differential scanning calorimetry (DSC) curves reveal that the glass-transition temperature (T_g) of CSE-R-P1 film is −1.04 °C, CSE-R-P2 film is −4.32 °C, and CSE-R-P3 film is −1.97 °C, respectively (Figures S48–S50, Supporting Information), indicating the soft behavior of all these CSE-RTP films at room temperature, as these lower T_g are beneficial for CSEs with improved tensile properties.

2.4. Multi-Level Anti-Counterfeiting Applications

The excellent dynamic chiral phosphorescence properties and mechanical characteristics of CSE-RTP allow for multiple potential applications. The multicolor CSE-RTP films with designed patterns show great potential in information encryption due to their fascinating optical properties, including reflection colors, RTP, time-dependent afterglow, and circular polarization characteristics, and mechanical stretching features. The schematic diagram of the information encryption device using CSE-RTP films with red-reflecting color is illustrated in **Figure 5**a, composed of right-handed CSE-P1(R-CSE-P1), right-handed CSE-P2 (R-CSE-P2), right-handed CSE-P3 (R-CSE-P3), left-handed CSE-P3 (L-CSE-P3), and right-handed CSE (R-CSE) materials. CSE-RTP films made of different patterns (such as multicolored flower, cube, and double-colored windmill patterns) are captured by

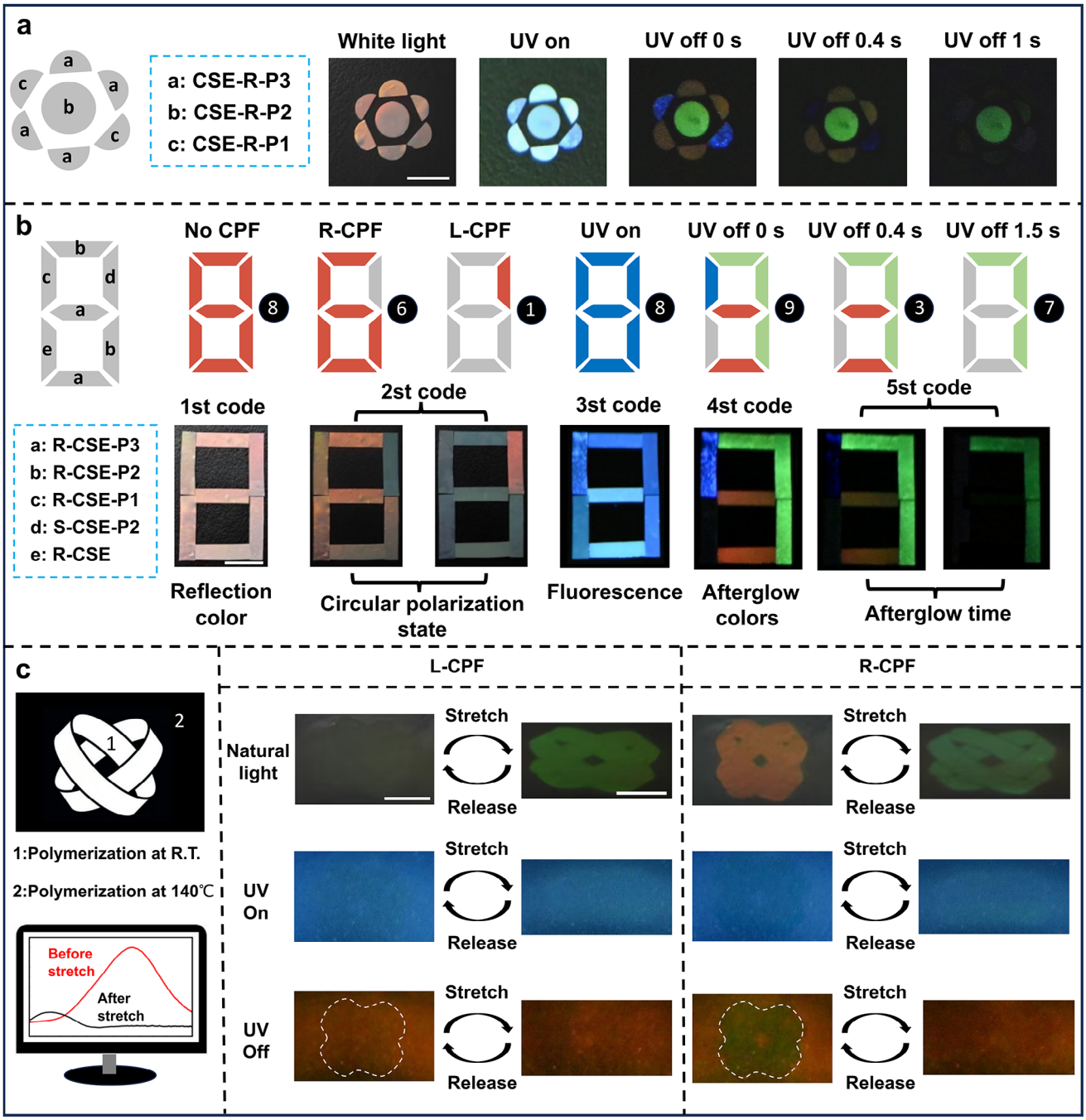

Figure 5. Multi-level information encryption of programmable CSE-RTP films. a) Photographs of colorful flower pattern based on different afterglow decay rates. b) Information encryption of number pattern. c) Dynamic information encryption and decryption based on mechanically-tunable CSE-RTP films. (scale bar = 1 cm).

switching UV light on and off (Figure 5a; Figure S51, Supporting Information). Initially, the as-prepared CSE-RTP films exhibit a red reflection color under white light distinguished by the naked eyes. When exposed to UV light, the cube and windmill patterns emit uniform blue fluorescence. After the UV light is turned off, the green and red afterglow emissions can be distinctly observed (Figure S51, Supporting Information). The flower pattern evolves dynamically, with blue disappearing first, followed by red, and finally green, due to the different afterglow decay rates of RTP polymers (Figure 5a). We also designed an anti-counterfeiting pattern of the digital number "8" by using different CSE-RTP films (Figure 5b). The number pattern includes the multi-level anti-counterfeiting features, each triggered by different optical states. The first level is designed under white light with no CPF, displaying the number "8" in red reflection; when a R-CPF is placed between the pattern and detector, the pattern displaying the number

"6" under white light becomes visible; while the number "1" is identified under L-CPF due to the variation in polarization states of the emitted CPL (second level). The third level is displayed when illuminated by 365 nm UV light under no CPF, showing blue fluorescence of number "8". After removing the UV irradiation, the number "9" is captured due to different afterglow colors of RTP polymers (fourth level). Subsequently, the number "3" and "7" become visible to the naked eyes in sequence, due to time-dependent afterglow of RTP polymers (fifth level). Thus, a number system pattern endowed with five optical states is fabricated, making the anti-counterfeiting application feasible.

In light of the unique mechanically-tunable CP-OURTP emissions, the device-oriented application of CSE-RTP films for dynamic information encryption is further explored. The encrypted information on CSE-RTP films can be rewritten and erased by using a customized photomask and UV light, showcasing a reversible photo-patterning behavior (Figure 5c). First, the desired information is encoded into CSE-RTP films via a "mobius ring" photomask for 5 min at room temperature, after which the photomask is removed and the remainder is polymerized at 140 °C at its isotropic state. The pattern of "mobius ring" with red reflection color can be observed under R-CPF in the initial state. The stretched patterned CSE-RTP film only demonstrates a green color under the R-CPF and shows dark under L-CPF at length strain of 20% because the patterned CSE-RTP film was initially structured as right-handed (Figure S52, Supporting Information). Whereas the green color of the patterned film can be observed under both R-CPF and L-CPF when the applied strain was 60% (Figure S52, Supporting Information). This is due to the fact that as the increase of the applied strain (when the strain length exceeds 40%), the helix deformations in CSE-RTP films gradually convert from a helical structure to a stratified structure, approaching a 1D Bragg reflector, and shift their optical state from right-handed circular polarization to unpolarized states that can reflect both left-handed and right-handed circularly polarized light. Under irradiation of UV light at 365 nm, the CSE-RTP film emits blue fluorescence, which is hardly distinguished by L-CPF and R-CPF before and after stretching. Notably, after turning off UV light, the pattern "mobius ring" shows red afterglow emission under L-CPF, whereas it emits green afterglow under R-CPF, corresponding to the red g_{lum} curve. After stretching, no obvious difference is detected under L-CPF and R-CPF for the "mobius ring" pattern, which agrees well with the minimum g_{lum} value (black curve). To assess the stability, repeatability, and long-term performance of our encryption device, particularly concerning its LPL properties, we conducted extended aging tests and repeated mechanical cycling experiments. Our observations reveal a high degree of operational stability. Specifically, after being stored under ambient conditions for over 30 days, the phosphorescence intensity of the encryption device remained virtually unchanged, exhibiting a negligible decrease, while the emission lifetime showed only a minor reduction (Figure S53, Supporting Information). This minimal degradation over an extended period strongly indicates the excellent long-term operational stability of the encryption device, particularly concerning its LPL functionality. Furthermore, to evaluate the device's performance under repeated use, we subjected it to tensile stretch-release cycles. Remarkably, even after 100 cycles of repeated mechanical actuation, the tensile stress-strain profiles of the encryption device showed no significant degradation, demonstrating its robust mechanical integrity (Figure S54, Supporting Information). Concurrently, we assessed the LPL performance after repeated stretching. In the initial, unstretched state, after multiple stretching cycles, we observed only modest degradations in phosphorescence intensity and in lifetime (Figure S55, Supporting Information). Under a higher strain of 100%, after repeated cycling, the degradations were slightly more pronounced in phosphorescence intensity and in lifetime (Figure S56, Supporting Information). These results collectively demonstrate that while some minor degradation in LPL performance is observed after extensive mechanical cycling, the overall impact of repeated stretching on the phosphorescence properties of the encryption device is remarkably limited. This robustness against both long-term storage and repeated mechanical deformation highlights the practical viability and potential for real-world applications of our persistent CP-OURTP encryption device. This excellent stability and durability, likely stemming from the robust encapsulation of the RTP polymers within the cross-linked CSE matrix,[17] positions our device favorably for applications requiring reliable and repeatable performance over extended periods and under mechanical stress. This pattern with the excellent processability provides new inspiration for fabricating novel CP-OURTP materials and demonstrates its applications in multi-level data encryption and decryption.

3. Conclusion

In summary, we successfully developed a strategy to construct the CSE-RTP films by using LC templates to self-assemble RTP polymers into chiral elastic polymer networks with reflection colors. The resulting CSE-RTP films exhibit remarkable chiroptical properties, such as circularly polarized structural colors under natural light, a dynamic and reversible control over g_{lum} ranging from 0.8 to 0.15, full-color afterglow emissions, and superior processability. The mechanically tunable CP-OURTP switching is achieved by the uniaxial stretching of CSE-RTP films due to the helix unwinding deformation, which influences the intrinsic circular polarization characteristics. As a proof-of-concept application, the as-developed CSE-RTP films can be applied to advanced information encryption. Based on characteristics of reflection colors, fluorescence, full-color afterglow emissions, time-dependent phosphorescence, and different polarization states, multi-level data encryption is demonstrated by using the fabricated CSE-RTP films. Furthermore, the construction of dynamic information encryption and decryption, which relies on the customized pattern encoded in CSE-RTP film, is enabled by mechanically tunable CP-OURTP. It is also demonstrated that the encrypted information as designed pattern can be rewritable and erasable on the CSE-RTP films using photomasks by mechanical deformation, showcasing reversible photo-patterning capabilities. This work can pave the way for the development of advanced CP-OURTP materials, opening up promising opportunities for their attractive applications in dynamic information encryption, flexible 3D displays and beyond.

4. Experimental Section

Materials: All commercially available chemicals and all solvents were purified before use. The polymerizable LC monomer (RM257), LC756,

EDDET, a photoinitiator (Irgacure 651), PETMP, and dipropylamine (DPA) were all acquired from the company of Nanjing Leyao Technology Co., LTD. The solvent dichloromethane (CH_2Cl_2) was provided by Macklin. The synthesis process of RTP polymers can be found in Supporting Information. LC glass substrates were acquired from the company of Kaiwei photoelectric technology in Zhuha. All Quartz substrates for CPL measurement were purchased from Prism Optics.

Preparation of CSE-R-P3 Film: LC monomer RM257 (71.2 wt.%) and chiral dopant LC756 (3.2 wt.%) were mixed in CH_2Cl_2 at room temperature for 5 min to form a homogeneous solution. Next, PETMP (4.8 wt.%), EDDET (18.5 wt.%), Irgacure 651 (0.55 wt.%), and RTP polymer with red emission (P3, 1.5 wt.%) were dissolved in CH_2Cl_2. Lastly, DPA (0.25 wt.%), serving as a catalyst, was first diluted to 1:50 ratio with CH_2Cl_2, and then added to the mixture. After stirring for 5 min, it was transferred to a glass petri dish (90 mm in diameter) and left open for 12 h to ensure the complete evaporation of the solvent. Last, the resulting CSE-RTP film was irradiated by UV light (365 nm, ≈50 mW cm^{-2}) for 10 min at 25 °C for the polymerization process. After polymerization, the CSE-R-P3 film was obtained.

Preparation of CSE-G-P2 Film: LC monomer RM257 (70.6 wt.%) and chiral dopant LC756 (3.8 wt.%) were mixed in CH_2Cl_2 at room temperature for 5 min to form a homogeneous solution. Next, PETMP (4.8 wt.%), EDDET (18.5 wt.%), Irgacure 651 (0.55 wt.%), and RTP polymer with green emission (P2, 1.5 wt.%) were dissolved in CH_2Cl_2. Lastly, DPA (0.25 wt.%), serving as a catalyst, was diluted to 1:50 ratio with CH_2Cl_2, and then added to the mixture. After stirring for 5 min, it was transferred to a glass petri dish (90 mm in diameter) and left open for 12 h to ensure the complete evaporation of the solvent. Last, the resulting CSE-RTP film was under UV light irradiation (365 nm, ≈50 mW cm^{-2}) for 10 min at 25 °C for the polymerization. After polymerization, the CSE-G-P2 film was obtained.

Preparation of CSE-B-P1 Film: LC monomer RM257 (70.2 wt.%) and the chiral dopant LC756 (4.2 wt.%) were mixed in CH_2Cl_2 at room temperature for 5 min to form a homogeneous solution. Next, PETMP (4.8 wt.%), EDDET (18.5 wt.%), Irgacure 651 (0.55 wt.%), and RTP polymer with blue emission (P3, 1.5 wt.%) were dissolved in CH_2Cl_2. Lastly, DPA (0.25 wt.%), serving as a catalyst, was diluted to 1:50 ratio with CH_2Cl_2, and then added to the mixture. After stirring for 5 min, it was transferred to a glass petri dish (90 mm in diameter) and left open for 12 h to ensure the complete evaporation of the solvent. Last, the resulting CSE-RTP film was under UV light irradiation (365 nm, ≈50 mW cm^{-2}) for 10 min at 25 °C for the polymerization process. After polymerization, the CSE-B-P1 film was obtained.

Spectroscopic Measurements: ^{1}HNMR (400 MHz) and ^{13}CNMR (100 MHz) spectra were measured using a Bruker ACF400 spectrometer at 298 K. The UV–visible absorption spectra were measured by Shimadzu UV-3600i PLUS. The steady-state fluorescence and phosphorescence spectra were measured using Hitachi F-4700. CSE-RTP films were characterized by using a Nikon camera. For microscopic observation, the samples were imaged using polarized optical microscopy (Nikon Ci-POL, Nikon company). CPL was characterized by circularly polarized luminometer (JASCO CPL-300). PL was measured by steady-state phosphorescence spectra (Hitachi F-4700). The lifetime curves were obtained on an Edinburgh FLS980 fluorescence spectrophotometer equipped with a Xenon arc lamp (Xe900) and a microsecond flash-lamp (uF900). Differential Scanning Calorimetry (DSC) was measured on NETZSCH DSC200F3 under nitrogen. Stress-strain measurements were performed on instron5942 by cutting the films with well-defined dimensions (length: 7 cm, width: 1 cm).

Supporting Information

Supporting Information is available from the Wiley Online Library or from the author.

Acknowledgements

The work was supported by the National Key R&D Program of China (Nos. 2022YFA1405000 and 2022YFA1204404), the National Natural Science Foundation of China (No. 62375141), the Natural Science Foundation of Jiangsu Province, Major Project (No. BK20243067), the National Natural Science Foundation of China (No. 62405142), the Natural Science Foundation of Jiangsu Province (No. BK20240656), the National Natural Science Foundation of China (No. 62405146), and the China Postdoctoral Science Foundation (2024M761391).

Conflict of Interest

The authors declare no conflict of interest.

Author Contributions

Z.P.S., J.W., and J.L. contributed equally to this work. Z.P.S., J.W., and J.L. contributed to the synthesis work, photophysical property study, and application study. Z.F.C., J.X.H., and S.C. analyzed data and revised the manuscript. Y.M., B.X.L., Y.Q.L., and Q.Z. wrote the manuscript and provided suggestions. All authors discussed the results and commented on the manuscript at all stages.

Data Availability Statement

The data that supports the findings of this study are available in the Supporting Information section of this article. Any other data are available from the corresponding authors upon request.

Keywords

chiral superstructure elastomer, circularly polarized luminescence, dissymmetry factor, multi-level information encryption, room-temperature phosphorescence

Received: December 14, 2024
Revised: March 5, 2025
Published online:

[1] X. Zhang, L. Li, Y. Chen, C. Valenzuela, Y. Liu, Y. Yang, Y. Feng, L. Wang, W. Feng, *Angew. Chem.* **2024**, *136*, 202404202.
[2] Y. He, S. Lin, J. Guo, Q. Li, *Aggregate* **2021**, *2*, 141.
[3] X. Yang, X. Gao, Y. X. Zheng, H. Kuang, C. F. Chen, M. Liu, P. Duan, Z. Tang, *CCS Chem.* **2023**, *5*, 2760.
[4] W. Kang, Y. Tang, X. Meng, S. Lin, X. Zhang, J. Guo, Q. Li, *Angew. Chem., Int. Ed.* **2023**, *62*, 202311486.
[5] S. Li, Y. Tang, Q. Fan, Z. Li, X. Zhang, J. Wang, J. Guo, Q. Li, *Light: Sci. Appl.* **2024**, *13*, 140.
[6] J. Qiao, Y. He, S. Lin, Q. Fan, J. Guo, *J. Mater. Chem. C* **2022**, *10*, 7311.
[7] J. Bao, R. Lan, C. Shen, R. Huang, Z. Wang, W. Hu, L. Zhang, H. Yang, *Adv. Opt. Mater.* **2021**, *10*, 2101910.
[8] Y. He, S. Zhang, H. K. Bisoyi, J. Qiao, H. Chen, J. Gao, J. Guo, Q. Li, *Angew. Chem., Int. Ed.* **2021**, *60*, 27158.
[9] J. Yan, F. Ota, B. A. San Jose, K. Akagi, *Adv. Funct. Mater.* **2016**, *27*, 1604529.
[10] Y. Sang, J. Han, T. Zhao, P. Duan, M. Liu, *Adv. Mater.* **2019**, *32*, 1900110.
[11] F. Yu, S. Liu, X. Liu, H. Zhang, Z. Zheng, W. H. Zhu, Y. Wu, *Adv. Opt. Mater.* **2024**, *12*, 2400411.
[12] Y. Wu, M. Li, Z. G. Zheng, Z. Q. Yu, W. H. Zhu, *J. Am. Chem. Soc.* **2023**, *145*, 12951.
[13] S. Liu, X. Liu, Y. Wu, D. Zhang, Y. Wu, H. Tian, Z. Zheng, W. H. Zhu, *Matter* **2022**, *5*, 2319.

[14] W. Lin, C. Yang, Y. Miao, S. Li, L. Zhang, X. F. Jiang, Y. Lv, B. Poudel, K. Wang, L. Polavarapu, C. Zhang, G. Zhou, X. Hu, *Adv. Mater.* **2023**, *35*, 2301573.
[15] H. Peng, G. Z. Xie, Y. Cao, L. Y. Zhang, L. Y. Zhang, X. Yan, X. Zhang, S. H. Miao, Y. Tao, H. H. Li, C. Zheng, W. Huang, R. F. Chen, *Sci. Adv.* **2022**, *8*, abk2925.
[16] J. Wei, C. Liu, J. Duan, A. Shao, J. Li, J. Li, W. Gu, Z. Li, S. Liu, Y. Ma, W. Huang, Q. Zhao, *Nat. Commun.* **2023**, *14*, 627.
[17] J. Wei, M. Zhu, T. Du, J. Li, P. Dai, C. Liu, J. Duan, S. Liu, X. Zhou, S. Zhang, L. Guo, H. Wang, Y. Ma, W. Huang, Q. Zhao, *Nat. Commun.* **2023**, *14*, 4839.
[18] W. Zhao, Z. He, B. Z. Tang, *Nat. Rev. Mater.* **2020**, *5*, 869.
[19] Z. An, C. Zheng, Y. Tao, R. Chen, H. Shi, T. Chen, Z. Wang, H. Li, R. Deng, X. Liu, W. Huang, *Nat. Mater.* **2015**, *14*, 685.
[20] X. W. Liu, W. Zhao, Y. Wu, Z. Meng, Z. He, X. Qi, Y. Ren, Z. Q. Yu, B. Z. Tang, *Nat. Commun.* **2022**, *13*, 3887.
[21] M. E. T. M. A. Baldo, S. R. Forrest, *Nature* **2000**, *403*, 750.
[22] J. Sun, H. Ahn, S. Kang, S. B. Ko, D. Song, H. A. Um, S. Kim, Y. Lee, P. Jeon, S. H. Hwang, Y. You, C. Chu, S. Kim, *Nat. Photonics* **2022**, *16*, 212.
[23] W. Ye, H. Ma, H. Shi, H. Wang, A. Lv, L. Bian, M. Zhang, C. Ma, K. Ling, M. Gu, Y. Mao, X. Yao, C. Gao, K. Shen, W. Jia, J. Zhi, S. Cai, Z. Song, J. Li, Y. Zhang, S. Lu, K. Liu, C. Dong, Q. Wang, Y. Zhou, W. Yao, Y. Zhang, H. Zhang, Z. Zhang, X. Hang, et al., *Nat. Mater.* **2021**, *20*, 1539.
[24] X. Zhang, M. Zeng, Y. Zhang, C. Zhang, Z. Gao, F. He, X. Xue, H. Li, P. Li, G. Xie, H. Li, X. Zhang, N. Guo, H. Cheng, A. Luo, W. Zhao, Y. Zhang, Y. Tao, R. Chen, W. Huang, *Nat. Commun.* **2023**, *14*, 475.
[25] Z. Huang, Z. He, B. Ding, H. Tian, X. Ma, *Nat. Commun.* **2022**, *13*, 7841.
[26] H. Li, J. Gu, Z. Wang, J. Wang, F. He, P. Li, Y. Tao, H. Li, G. Xie, W. Huang, C. Zheng, R. Chen, *Nat. Commun.* **2022**, *13*, 429.
[27] M. Zeng, W. Wang, S. Zhang, Z. Gao, Y. Yan, Y. Liu, Y. Qi, X. Yan, W. Zhao, X. Zhang, N. Guo, H. Li, H. Li, G. Xie, Y. Tao, R. Chen, W. Huang, *Nat. Commun.* **2024**, *15*, 3053.
[28] M. Cao, Y. Ren, Y. Wu, J. Shen, S. Li, Z. Q. Yu, S. Liu, J. Li, O. J. Rojas, Z. Chen, *Nat. Commun.* **2024**, *15*, 2375.
[29] L. Gu, W. Ye, X. Liang, A. Lv, H. Ma, M. Singh, W. Jia, Z. Shen, Y. Guo, Y. Gao, H. Chen, D. Wang, Y. Wu, J. Liu, H. Wang, Y. X. Zheng, Z. An, W. Huang, Y. Zhao, *J. Am. Chem. Soc.* **2021**, *143*, 18527.
[30] J. Liu, Z. P. Song, J. Wei, J. J. Wu, M. Z. Wang, J. G. Li, Y. Ma, B. X. Li, Y. Q. Lu, Q. Zhao, *Adv. Mater.* **2024**, *36*, 2306834.
[31] K. Jiang, Q. Fan, D. Guo, C. Song, J. Guo, *ACS Appl. Mater. Interfaces* **2023**, *15*, 26037.
[32] X. Wang, B. Zhao, J. Deng, *Adv. Mater.* **2023**, *35*, 2304405.
[33] M. Yang, Y. Xu, X. Zhang, H. K. Bisoyi, P. Xue, Y. Yang, X. Yang, C. Valenzuela, Y. Chen, L. Wang, W. Feng, Q. Li, *Adv. Funct. Mater.* **2022**, *32*, 2201884.
[34] Q. Fan, Y. Tang, H. Sun, D. Guo, J. Ma, J. Guo, *Adv. Mater.* **2024**, *36*, 2401315.
[35] J. Ma, Y. Yang, C. Valenzuela, X. Zhang, L. Wang, W. Feng, *Angew. Chem., Int. Ed.* **2022**, *61*, 202116219.
[36] H. K. Bisoyi, Q. Li, *Chem. Rev.* **2021**, *122*, 4887.
[37] X. Yang, C. Valenzuela, X. Zhang, Y. Chen, Y. Yang, L. Wang, W. Feng, *Matter* **2023**, *6*, 1278.
[38] Y. L. Yu, T. Maeda, J. I. Mamiya, T. Ikeda, *Angew. Chem., Int. Ed.* **2007**, *46*, 881.
[39] J. Gao, M. Tian, Y. He, H. Yi, J. Guo, *Adv. Funct. Mater.* **2021**, *32*, 2107145.
[40] Q. Fan, Z. Li, K. Jiang, J. Gao, S. Lin, J. Guo, *Cell Rep. Phys. Sci.* **2023**, *4*, 101583.
[41] S. Lin, T. Ren, X. Meng, W. Kang, J. Guo, *Sci. China Chem.* **2024**, *67*, 2719.
[42] C. Kwon, S. Nam, S. H. Han, S. S. Choi, *Adv. Funct. Mater.* **2023**, *33*, 2304506.
[43] A. Juan, H. Sun, J. Qiao, J. Guo, *Chem. Commun.* **2020**, *56*, 13649.
[44] R. Kizhakidathazhath, Y. Geng, V. S. R. Jampani, C. Charni, A. Sharma, J. P. F. Lagerwall, *Adv. Funct. Mater.* **2019**, *30*, 1909537.
[45] A. M. Martinez, M. K. McBride, T. J. White, C. N. Bowman, *Adv. Funct. Mater.* **2020**, *30*, 2003150.
[46] J. Choi, Y. Choi, J. H. Lee, M. C. Kim, S. Park, K. Hyun, K. M. Lee, T. H. Yoon, S. k. Ahn, *Adv. Funct. Mater.* **2023**, *34*, 2310658.
[47] P. Cicuta, A. R. Tajbakhsh, E. M. Terentjev, *Phys. Rev. E* **2004**, *70*, 011703.
[48] Y. S. Jo, T. H. Choi, S. M. Ji, T. H. Yoon, *AIP Adv.* **2018**, *8*, 085004.
[49] C. L. C. Chan, M. M. Bay, G. Jacucci, R. Vadrucci, C. A. Williams, G. T. van de Kerkhof, R. M. Parker, K. Vynck, B. Frka Petesic, S. Vignolini, *Adv. Mater.* **2019**, *31*, 1905151.
[50] J. H. Shin, H. J. Yang, J. Y. Park, S. H. Han, D. Kim, S. Nam, S. S. Choi, *Adv. Funct. Mater.* **2024**, 2422772.